Nuclear Engineering and Technology 57 (2025) 103753

Contents lists available at ScienceDirect

Nuclear Engineering and Technology

journal homepage: www.elsevier.com/locate/net

Original Article

Impact of representative ground motion level on seismic PSA with the boundary between overestimation and underestimation

Jisuk Kim [a], Man Cheol Kim [b,*]

[a] Idaho National Laboratory, 2525 North Fremont Avenue, Idaho Falls, ID, USA
[b] Chung-Ang University, 84 Heukseok-ro, Dongjak-gu, Seoul, South Korea

ARTICLE INFO

Keywords:
Seismic probabilistic safety assessment
Quantification
Discrete approach
Representative ground motion level

ABSTRACT

One commonly used approach to seismic probabilistic safety assessment (PSA) is the discrete method, which follows the conventional PSA framework and can be applied to various different model types (e.g., multi-unit models). As it is performed using standard software, this method reduces computational costs. However, as intervals cannot be subdivided infinitely, the discrete method instead utilizes an approximation based on a finite number of subintervals. In practice, different numbers of subinterval are applied, and the representative ground motion level is selected based on expert judgment. When employing a smaller number of subintervals, care must be taken to prevent underestimation of risk. The present study analyzes the impact of representative ground motion level on seismic risk, confirming that underestimation can indeed occur with a small number of subintervals, depending on the representative ground motion level. Specifically, using the left endpoint underestimates, the right endpoint overestimates, and the midpoint may do either. It also proposes a method for determining the underestimation-overestimation boundary. This method is demonstrated via examples, affording a mathematical basis for the appropriate selection of representative ground motion levels. Avoiding underestimation helps prevent significant risk contributors from being overlooked and enhances the current understanding of seismic risk.

1. Introduction

Probabilistic Safety Assessment (PSA) is an integrated, structured approach to quantitatively evaluate the risk from nuclear power plants. It tries to answer what can go wrong, what the consequences are, and how likely it is. Recent improvements in conventional PSA include the frequency calculation of interfacing system loss of coolant accident [1] and state-of-knowledge correlation effect [2]. Multi-unit PSA [3] and dynamic PSA [4–7] have also been widely investigated.

Seismic PSA is a component of PSA to evaluate the risk that seismic events pose to nuclear power plants. Seismic PSA generally consists of seismic hazard analysis, seismic fragility analysis, systems analysis, and quantification [8–10]. The seismic hazard analysis generates seismic hazard curves that indicate the exceedance frequencies of ground motion levels, along with the uncertainties that correspond to those frequencies. Seismic fragility analysis gives the seismic fragility probabilities of systems, structures, and components (SSCs). Both types of analyses are required input for determining the risk posed by seismic events, as opposed to that posed by general internal events. Systems analysis enables a logic model to be generated in the wake of a seismic initiating event, with event and fault trees that consider seismic failures of SSCs [11]. In the quantification process for seismic PSA, a nuclear power plant's core damage frequency initiated by a seismic event is calculated per the convolution of the hazard and fragility curves. Recently, multi-unit seismic PSA has also been investigated [12].

There are various approaches to quantifying the seismic PSA. Kwag et al. [37] categorized them as either complete sampling, semi-sampling, or analytical methods, while Zhou et al. [10] categorized them into two numerical schemes: simulation based and discretization based. The simulation-based scheme combines the seismic hazard and fragility curves by sampling random variables via Monte Carlo simulation and Latin hypercube sampling. The sampling and semi-sampling approach can be considered as part of the simulation-based scheme. Various studies have been conducted using simulation-based approaches, and Monte-Carlo-based direct quantification of fault trees is an example of one such approach that is currently experiencing active utilization and enhancement ([13,14,15,37,]). Although this method can consider seismic correlations, sufficient sampling is required for accurate results,

* Corresponding author.
E-mail address: charleskim@cau.ac.kr (M.C. Kim).

https://doi.org/10.1016/j.net.2025.103753
Received 13 February 2025; Received in revised form 5 June 2025; Accepted 13 June 2025
Available online 14 June 2025

thus leading to high computational costs. Another method is a discrete approach based on discretization of the continuous distribution, which is considered as an analytical method and is the primary focus of this study [9,10,16]. In this method, the ground motion level (e.g., peak ground acceleration and spectral acceleration) is discretized into several subintervals. The seismic risk is then analyzed by assuming a representative ground motion level for each. Since the discrete approach follows the conventional PSA framework, a number of guidelines on seismic PSA describe this approach [9,17,18]. In addition, the analysis can be performed without great computational effort, using standard software. Furthermore, active research is being conducted on hybrid methods that consider both the simulation and discrete approaches. Zhou et al. [10] accounted for dependencies between multi-unit SSCs by considering a combination of parallel Monte Carlo simulations and discrete approaches.

However, even if the conventional PSA framework is employed for the discrete approach, applying the existing quantification method may inject a large amount of uncertainty into the results of seismic events. This is because undue conservatism can be injected when employing rare event approximations and minimal cut-set upper bounds, as are typically used to quantify internal events. Han [19] introduced a method of partially performing binary decision diagram calculations to increase the quantification accuracy. Park and Jung [20] introduced a new quantification method called "probability subtraction" to avoid overestimation of the risk. Jung [21] identified the effect of underestimation when combinations of mutually exclusive events are not deleted, and suggested a method of explicitly accounting for conditional events in a fault tree so as to avoid this issue. And Kim and Kim [22] provided insights into the quantification of seismic risk by using approximations such as the delete-term approximation, rare event approximation, and minimal cut-set upper bound while applying the negate-down, which is a new feature in seismic quantification.

In addition, the number of subintervals and the representative ground motion level should be carefully selected. Kim and Kim [23] showed that accuracy improves as the number of subintervals increases. However, in practical applications, it is unrealistic to subdivide the intervals infinitely due to computational constraints, as each subinterval requires a seismic PSA model and evaluation process. They also showed that underestimation can occur when the number of subintervals is small [24]. Furthermore, the number of subintervals and the representative ground motion levels are applied differently depending on the application. For example, 8, 9, and 16 subintervals of ground motion level were employed in the seismic PSAs performed on the Surry [25], Sequoyah [26], and Diablo Canyon [27] plants, respectively. And although Zhou et al. [10] showed that geometric ground motion level produces non-conservative results, there remains a lack of clarity as to what specific value to select for the ground motion level. In addition, the discrete approach inherently introduces interpolation errors when estimating seismic responses between seismic intensity levels [28,29].

Many studies have been conducted to reduce uncertainty and produce more accurate results by avoiding conservatism or the underestimation of seismic risk. This study focuses on the representative ground motion level in the discrete approach, which has historically been assumed without sufficient justification. The aim of this study is to analyze the effect of representative ground motion level on seismic risk and to provide a mathematical background for selecting the appropriate level in practice. Section 2 discusses practical application of the discrete approach's convolution of the hazard and fragility curves. Section 3 mathematically demonstrates how the representative ground motion level affects seismic risk estimations. Section 4 introduces a method for deriving the boundary between overestimating and underestimating seismic risk. Section 5 examines the applicability of this method in the context of a specific example. The outcomes of this study are discussed in Section 6, and the overall conclusions are presented in Section 7.

2. Discrete approach to seismic quantification in practice

By integrating the convolution (i.e., product) of the hazard and fragility curves, we can obtain the seismic risk. In theory, all ground motion levels should be considered; however, in actual seismic PSA practice, only a specific range is covered, as SSCs are designed to withstand both the operating basis earthquake and the safe shutdown earthquake. For higher ground motion levels, direct core damage is generally assumed, without the need for detailed analysis.

The seismic risk stemming from the ground motion levels a to b can be obtained per:

$$P = \int_a^b -\frac{dH(x)}{dx} F(x)dx \tag{1}$$

where $H(x)$ is a hazard curve and $F(x)$ is a fragility curve for the ground motion level x. The hazard curve represents the rate of earthquakes exceeding ground motion level. This curve, which is generally decreasing, can be approximated via Eq. (2) if using an appropriate constant (K_I) and slope parameter (K_H) [30,31]. The fragility curve represents the failure probability of an SSC, and per Eq. (3) it is generally assumed to be lognormally distributed with a median capacity ground motion level (A_m) and a composite standard deviation (β_c) [32]. The composite standard deviation (β_c) can be calculated by taking the square of the sum of the aleatory standard deviation (β_r) and epistemic standard deviation (β_u).

$$H(x) = K_I x^{-K_H} \tag{2}$$

$$F(x) = \Phi\left(\frac{\ln(x) - \ln(A_m)}{\beta_c}\right) \tag{3}$$

In the discrete approach, seismic risk is quantified by several subintervals, as per:

$$P = \lim_{\substack{N\to\infty \\ (\Delta x\to 0)}} \sum_{i=1}^{N} \frac{H(x_i) - H(x_i + \Delta x)}{\Delta x} F(x_i)\Delta x \tag{4}$$

where N is the number of subintervals and Δx is the length of the subintervals when the ground motion level discretizes into equally spaced subintervals from a to b.

If the number of subintervals extends to infinity, the exact risk can be obtained. However, in actual application, the PSA model should be developed the same number of times as the subintervals are discretized. Thus, the number of subintervals is instead considered to be finite and the seismic risk is approximated using the Riemann sum. The approximated seismic risk is defined by Eq. (5)—an approach commonly used in practice [9,18,33]:

$$P \approx \sum_{i=1}^{N} (H(x_i) - H(x_i + \Delta x))F(x_i) \tag{5}$$

On the other hand, the different representative ground motion levels can be applied in the hazard and fragility terms, as per:

$$P \approx \sum_{i=1}^{N} (H(x_{h(i)}) - H(x_{h(i+1)}))F(x_{f(i)}) \tag{6}$$

where $x_{h(i)}$ and $x_{f(i)}$ denote the representative ground motion levels within the i-th subinterval for the hazard and fragility curves, respectively. Since the earthquake occurrence frequency is derived by determining the difference between the exceeding frequency from the hazard curve, $x_{h(i)}$ is usually assumed to be the left endpoints of the ground motion level within the subintervals. Alternatively, $x_{h(i+1)}$ can be expressed as $x_{h(i)} + \Delta x$. However, $x_{f(i)}$ can be assumed to be either the left endpoint, right endpoint, or midpoint level within the subintervals. The effect of the number of subintervals can differ depending on the setting value of $x_{f(i)}$, as explained in Section 3.

3. Effect of representative ground motion level on seismic risk

This section analyzes the effect that the number of subintervals has on seismic risk, depending on the representative ground motion level. Specifically, as regards the representative ground motion level of the fragility curve, there are three possibilities: it is assumed to be either at the left endpoint, right endpoint, or midpoint level within the subinterval.

The seismic risk from the ground motion level a to b, as approximated via Eq. (5), is denoted by $P_{u,v}$, where u denotes the representative ground motion level for the fragility curve, which corresponds to the left endpoint (l), right endpoint (r), and midpoint (m) level; v denotes the number of subintervals, with the ground motion level being discretized by 2^n and 2^{n+1}, as represented by $\{1,2\}$, respectively; and the indices are defined as $u \in \{l,r,m\}$ and $v \in \{1,2\}$.

The representative ground motion levels of the hazard curve are assumed to be left endpoints, so the hazard term of the approximation in Eq. (5) equates to the change in the hazard—from the minimum to the maximum level—within the subintervals. Thus, $x_{h(i)}$ and $x_{h(i+1)}$ of the hazard term are applied to the left endpoint of the i-th and $i+$ 1-th subinterval—namely, $a+(i-1)\Delta x$ and $a+i\Delta x$.

3.1. Seismic risk for the left endpoint of the fragility curve within the subinterval

The seismic risk, as denoted by $P_{u=l}$, was approximated by assuming the representative ground motion level of the fragility curve to be the left endpoint within the subinterval from Eq. (6). Per Eq. (7), $x_{f(i)}$ was applied to the left endpoint of the i-th subinterval, which is $a+$ $(i-1)\Delta x$.

$$P_{u=l}=\sum_{i=1}^{N}(H(a+(\mathrm{i}-1)\Delta x)-H(a+i\Delta x))F(a+(i-1)\Delta x) \tag{7}$$

To compare seismic risk depending on the number of subintervals, we defined the seismic risk $P_{l,1}$ and $P_{l,2}$ by utilizing Eqs. (8) and (9), which are discretized by 2^n and 2^{n+1}, respectively.

$$P_{l,1}=\sum_{i=1}^{2^n}\left(H\left(a+\frac{(i-1)(b-a)}{2^n}\right)-H\left(a+\frac{i(b-a)}{2^n}\right)\right)F\left(a+\frac{(i-1)(b-a)}{2^n}\right) \tag{8}$$

$$P_{l,2}=\sum_{j=1}^{2^{n+1}}\left(H\left(a+\frac{(j-1)(b-a)}{2^{n+1}}\right)-H\left(a+\frac{j(b-a)}{2^{n+1}}\right)\right)F\left(a+\frac{(j-1)(b-a)}{2^{n+1}}\right) \tag{9}$$

The seismic risk $P_{l,2}$ can be transformed by Eq. (10) to be equal to the upper bound of the summation in Eq. (8).

$$\begin{aligned}P_{l,2}=\sum_{i=1}^{2^n}&\left(\left(H\left(a+\frac{(2i-2)(b-a)}{2^{n+1}}\right)-H\left(a+\frac{(2i-1)(b-a)}{2^{n+1}}\right)\right)\right.\\&F\left(a+\frac{(2i-2)(b-a)}{2^{n+1}}\right)+\left(H\left(a+\frac{(2i-1)(b-a)}{2^{n+1}}\right)\right.\\&\left.\left.-H\left(a+\frac{2i(b-a)}{2^{n+1}}\right)\right)F\left(a+\frac{(2i-1)(b-a)}{2^{n+1}}\right)\right)\end{aligned} \tag{10}$$

Since the index and the upper bound of summation of Eq. (10) matches up with those of Eq. (8), the two summations from Eq. (8) and Eq. (10) can be combined into a single summation. By using Eq. (11), we can compare $P_{l,1}$ and $P_{l,2}$.

$$\begin{aligned}P_{l,1}-P_{l,2}=\sum_{i=1}^{2^n}&\left(H\left(a+\frac{(i-1)(b-a)}{2^n}\right)-H\left(a+\frac{i(b-a)}{2^n}\right)\right)\\&F\left(a+\frac{(i-1)(b-a)}{2^n}\right)-\sum_{i=1}^{2^n}\left(\left(H\left(a+\frac{(2i-2)(b-a)}{2^{n+1}}\right)\right.\right.\\&\left.-H\left(a+\frac{(2i-1)(b-a)}{2^{n+1}}\right)\right)F\left(a+\frac{(2i-2)(b-a)}{2^{n+1}}\right)\\&+\left(H\left(a+\frac{(2i-1)(b-a)}{2^{n+1}}\right)-H\left(a+\frac{2i(b-a)}{2^{n+1}}\right)\right)\\&\left.F\left(a+\frac{(2i-1)(b-a)}{2^{n+1}}\right)\right)\end{aligned} \tag{11}$$

Eq. (11) is simplified into Eq. (12) via summation of the factorized equation.

$$\begin{aligned}P_{l,1}-P_{l,2}=\sum_{i=1}^{2^n}&\left(H\left(a+\frac{(2i-1)(b-a)}{2^{n+1}}\right)-H\left(a+\frac{2i(b-a)}{2^{n+1}}\right)\right)\\&\left(F\left(a+\frac{(2i-2)(b-a)}{2^{n+1}}\right)-F\left(a+\frac{(2i-1)(b-a)}{2^{n+1}}\right)\right)\end{aligned} \tag{12}$$

The inequalities shown below in Eq. (13) are always satisfied because the typical hazard curve is a decreasing one, and the typical fragility curve is an increasing one. Accordingly, the hazard term in Eq. (12) is always positive and the fragility term always negative.

$$\begin{cases}H\left(a+\frac{(2i-2)(b-a)}{2^{n+1}}\right)>H\left(a+\frac{(2i-1)(b-a)}{2^{n+1}}\right)>H\left(a+\frac{2i(b-a)}{2^{n+1}}\right)\\F\left(a+\frac{(2i-2)(b-a)}{2^{n+1}}\right)<F\left(a+\frac{(2i-1)(b-a)}{2^{n+1}}\right)<F\left(a+\frac{2i(b-a)}{2^{n+1}}\right)\end{cases} \tag{13}$$

Therefore, Eq. (12) always has a negative value when the representative ground motion level of the fragility curve is assumed to be the left endpoint within the subintervals. This means greater seismic risk stems from a larger number of subintervals than from a smaller number. In other words, an insufficient number of subintervals may lead to underestimation of risk.

3.2. Seismic risk for the right endpoint of the fragility curve within the subinterval

The seismic risk was also approximated by assuming the representative ground motion level for the fragility curve to be the right endpoint within the i-th subinterval, which is $a+i\Delta x$, and denoted by $P_{u=r}$. The seismic risk based on the right endpoint is defined by Eq. (14), and is discretized by 2^n and 2^{n+1} in Eqs. (15) and (16), respectively.

$$P_{u=r}=\sum_{i=1}^{N}(H(a+(\mathrm{i}-1)\Delta x)-H(a+i\Delta x))F(a+i\Delta x) \tag{14}$$

$$P_{r,1}=\sum_{i=1}^{2^n}\left(H\left(a+\frac{(i-1)(b-a)}{2^n}\right)-H\left(a+\frac{i(b-a)}{2^n}\right)\right)F\left(a+\frac{i(b-a)}{2^n}\right) \tag{15}$$

$$P_{r,2}=\sum_{j=1}^{2^{n+1}}\left(H\left(a+\frac{(j-1)(b-a)}{2^{n+1}}\right)-H\left(a+\frac{j(b-a)}{2^{n+1}}\right)\right)F\left(a+\frac{j(b-a)}{2^{n+1}}\right) \tag{16}$$

Similarly, the seismic risk $P_{r,2}$ can be transformed by adjusting the upper bound of the summation from Eq. (16), as per:

$$P_{r,2}=\sum_{i=1}^{2^n}\left(\left(H\left(a+\frac{(2i-2)(b-a)}{2^{n+1}}\right)-H\left(a+\frac{(2i-1)(b-a)}{2^{n+1}}\right)\right)\right.$$
$$F\left(a+\frac{(2i-1)(b-a)}{2^{n+1}}\right)+\left(H\left(a+\frac{(2i-1)(b-a)}{2^{n+1}}\right)-H\left(a+\frac{2i(b-a)}{2^{n+1}}\right)\right)$$
$$\left.F\left(a+\frac{2i(b-a)}{2^{n+1}}\right)\right) \tag{17}$$

The following equation can be used to compare $P_{r,1}$ and $P_{r,2}$:

$$P_{r,1}-P_{r,2}=\sum_{i=1}^{2^n}\left(H\left(a+\frac{(i-1)(b-a)}{2^n}\right)-H\left(a+\frac{i(b-a)}{2^n}\right)\right)$$
$$F\left(a+\frac{i(b-a)}{2^n}\right)$$
$$-\sum_{i=1}^{2^n}\left(\left(H\left(a+\frac{(2i-2)(b-a)}{2^{n+1}}\right)-H\left(a+\frac{(2i-1)(b-a)}{2^{n+1}}\right)\right)\right.$$
$$F\left(a+\frac{(2i-1)(b-a)}{2^{n+1}}\right)+\left(H\left(a+\frac{(2i-1)(b-a)}{2^{n+1}}\right)-H\left(a+\frac{2i(b-a)}{2^{n+1}}\right)\right)$$
$$\left.F\left(a+\frac{2i(b-a)}{2^{n+1}}\right)\right) \tag{18}$$

Similar to the previous process, Eq. (18) can be transformed into Eq. (19):

$$P_{r,1}-P_{r,2}=\sum_{i=1}^{2^n}\left(\left(H\left(a+\frac{(2i-2)(b-a)}{2^{n+1}}\right)-H\left(a+\frac{(2i-1)(b-a)}{2^{n+1}}\right)\right)\right.$$
$$\left.\left(F\left(a+\frac{2i(b-a)}{2^{n+1}}\right)-F\left(a+\frac{(2i-1)(b-a)}{2^{n+1}}\right)\right)\right) \tag{19}$$

Due to the properties of the hazard and fragility curves in Eq. (13), the hazard and fragility terms of Eq. (19) are always positive. Accordingly, the seismic risk discretized by 2^n exceeds the risk discretized by 2^{n+1}, meaning that a small number of discretization cannot cause underestimation.

3.3. Seismic risk for the midpoint of the fragility curve within the subinterval

Finally, the seismic risk was approximated by assuming the representative ground motion level for the fragility curve to be the midpoint within the i-th subinterval, which is $a+\frac{(2i-1)}{2}\Delta x$, and denoted by $P_{u=m}$. The seismic risk based on the midpoint level is defined as:

$$P_{u=m}=\sum_{i=1}^{N}(H(a+(i-1)\Delta x)-H(a+i\Delta x))F\left(a+\frac{(2i-1)}{2}\Delta x\right) \tag{20}$$

When the number of subintervals is 2^n, the seismic risk can be calculated using Eq. (21). The hazard term can be expanded because the sum of the hazard terms is the same regardless of number of subintervals.

$$P_{m,1}=\sum_{i=1}^{2^n}\left(\left(H\left(a+\frac{(i-1)(b-a)}{2^n}\right)-H\left(a+\frac{i(b-a)}{2^n}\right)\right)\right.$$
$$\left.F\left(a+\frac{(2i-1)(b-a)}{2^{n+1}}\right)\right)=\sum_{i=1}^{2^n}\left(\left(H\left(a+\frac{(2i-2)(b-a)}{2^{n+1}}\right)\right.\right.$$
$$\left.-H\left(a+\frac{(2i-1)(b-a)}{2^{n+1}}\right)\right)F\left(a+\frac{(2i-1)(b-a)}{2^{n+1}}\right)$$
$$+\left(H\left(a+\frac{(2i-1)(b-a)}{2^{n+1}}\right)-H\left(a+\frac{2i(b-a)}{2^{n+1}}\right)\right)F\left(a+\frac{(2i-1)(b-a)}{2^{n+1}}\right)\Bigg) \tag{21}$$

When the number of subintervals is 2^{n+1}, the seismic risk can be calculated via Eq. (22) and transformed by adjusting the upper bound of the summation.

$$P_{m,2}=\sum_{j=1}^{2^{n+1}}\left(\left(H\left(a+\frac{(j-1)(b-a)}{2^{n+1}}\right)-H\left(a+\frac{j(b-a)}{2^{n+1}}\right)\right)\right.$$
$$\left.F\left(a+\frac{(2j-1)(b-a)}{2^{n+2}}\right)\right)=\sum_{i=1}^{2^n}\left(\left(H\left(a+\frac{(2i-2)(b-a)}{2^{n+1}}\right)\right.\right.$$
$$\left.-H\left(a+\frac{(2i-1)(b-a)}{2^{n+1}}\right)\right)F\left(a+\frac{(4i-3)(b-a)}{2^{n+2}}\right)$$
$$+\left(H\left(a+\frac{(2i-1)(b-a)}{2^{n+1}}\right)-H\left(a+\frac{2i(b-a)}{2^{n+1}}\right)\right)F\left(a+\frac{(4i-1)(b-a)}{2^{n+2}}\right)\Bigg) \tag{22}$$

The equation for comparing $P_{m,1}$ and $P_{m,2}$ can be defined by Eq. (23) and manipulated in its simplest form.

$$P_{m,1}-P_{m,2}=\sum_{i=1}^{2^n}\left(\left(H\left(a+\frac{(2i-2)(b-a)}{2^{n+1}}\right)-H\left(a+\frac{(2i-1)(b-a)}{2^{n+1}}\right)\right)\right.$$
$$\left(F\left(a+\frac{(4i-2)(b-a)}{2^{n+2}}\right)-F\left(a+\frac{(4i-3)(b-a)}{2^{n+2}}\right)\right)$$
$$+\left(H\left(a+\frac{(2i-1)(b-a)}{2^{n+1}}\right)-H\left(a+\frac{2i(b-a)}{2^{n+1}}\right)\right)$$
$$\left.\left(F\left(a+\frac{(4i-2)(b-a)}{2^{n+2}}\right)-F\left(a+\frac{(4i-1)(b-a)}{2^{n+2}}\right)\right)\right) \tag{23}$$

Because the typical hazard curve is generally decreasing convex, the inequalities shown in Eq. (24) and Eq. (13) are satisfied. Accordingly, the hazard terms are always positive, and the first term of the hazard exceeds the second term, as shown in Eq. (25).

$$H\left(a+\frac{(2i-1)(b-a)}{2^{n+1}}\right)<\frac{H\left(a+\frac{(2i-2)(b-a)}{2^{n+1}}\right)+H\left(a+\frac{2i(b-a)}{2^{n+1}}\right)}{2} \tag{24}$$

$$H\left(a+\frac{(2i-2)(b-a)}{2^{n+1}}\right)-H\left(a+\frac{(2i-1)(b-a)}{2^{n+1}}\right)>H\left(a+\frac{(2i-1)(b-a)}{2^{n+1}}\right)$$
$$-H\left(a+\frac{2i(b-a)}{2^{n+1}}\right) \tag{25}$$

The fragility curve is satisfied as regards the inequality reflected in Eq. (26) because it is an increasing curve. The first term of the fragility curve in Eq. (23) is positive but the second is negative.

$$F\left(a+\frac{(4i-3)(b-a)}{2^{n+2}}\right)<F\left(a+\frac{(4i-2)(b-a)}{2^{n+2}}\right)<F\left(a+\frac{(4i-1)(b-a)}{2^{n+2}}\right) \tag{26}$$

Additionally, the fragility curve has both convex and concave regions. In the concave region, which has a higher ground motion level, Eq. (27) is satisfied. Because of the property of the concave curve, the first term of the fragility curve exceeds the second, as shown in Eq. (28).

$$F\left(a+\frac{(4i-2)(b-a)}{2^{n+2}}\right)>\frac{F\left(a+\frac{(4i-3)(b-a)}{2^{n+2}}\right)+F\left(a+\frac{(4i-1)(b-a)}{2^{n+2}}\right)}{2} \tag{27}$$

$$F\left(a+\frac{(4i-2)(b-a)}{2^{n+2}}\right)-F\left(a+\frac{(4i-3)(b-a)}{2^{n+2}}\right)$$
$$>F\left(a+\frac{(4i-1)(b-a)}{2^{n+2}}\right)-F\left(a+\frac{(4i-2)(b-a)}{2^{n+2}}\right) \tag{28}$$

Eqs. (25) and (28) can be summarized by Eq. (29), and Eq. (23) can be confirmed to always be positive, since the absolute value of the negative term of Eq. (23) is less than that of the positive term of Eq. (23) via Eq. (29). That is, as the number of subintervals increases, the seismic risk decreases in the concave region of the fragility curve.

$$\left(H\left(a+\frac{(2i-1)(b-a)}{2^{n+1}}\right)-H\left(a+\frac{2i(b-a)}{2^{n+1}}\right)\right)\left(F\left(a+\frac{(4i-1)(b-a)}{2^{n+2}}\right)-F\left(a+\frac{(4i-2)(b-a)}{2^{n+2}}\right)\right)<\left(H\left(a+\frac{(2i-2)(b-a)}{2^{n+1}}\right)-H\left(a+\frac{(2i-1)(b-a)}{2^{n+1}}\right)\right)\left(F\left(a+\frac{(4i-2)(b-a)}{2^{n+2}}\right)-F\left(a+\frac{(4i-3)(b-a)}{2^{n+2}}\right)\right) \tag{29}$$

On the other hand, it is not satisfied in the convex region of the fragility curve. If the hazard curve is linear, the hazard terms of Eq. (23) are identical as well as positive. Eq. (23) can then be transformed into Eq. (30), and the seismic risk is affected solely by the fragility curve. Eq. (30) is always negative because of the convex property, as shown in Eq (31). Thus, the seismic risk might be underestimated as the number of subintervals decreases in the convex region of the linear hazard curve.

$$P_{m,1}-P_{m,2}=\sum_{i=1}^{2^n}\left(H\left(a+\frac{(2i-2)(b-a)}{2^{n+1}}\right)-H\left(a+\frac{(2i-1)(b-a)}{2^{n+1}}\right)\right)\left(2F\left(a+\frac{(4i-2)(b-a)}{2^{n+2}}\right)-F\left(a+\frac{(4i-3)(b-a)}{2^{n+2}}\right)-F\left(a+\frac{(4i-1)(b-a)}{2^{n+2}}\right)\right) \tag{30}$$

$$F\left(a+\frac{(4i-2)(b-a)}{2^{n+2}}\right)<\frac{F\left(a+\frac{(4i-3)(b-a)}{2^{n+2}}\right)+F\left(a+\frac{(4i-1)(b-a)}{2^{n+2}}\right)}{2} \tag{31}$$

However, since the hazard curve is decreasing convex rather than linear, the underestimation results stemmed from the lower ground motion level of the fragility curve's convex region. The seismic risks depending on the number of subintervals were compared based on whether Eq. (23) was negative or positive. For instance, Eq. (23) being negative meant that the seismic risk with 2^n subintervals was less than the risk with 2^{n+1}. The boundary for the result depends on the ratios of the hazard and fragility differences, which are derived from Eq. (23), as follows:

$$\begin{cases}\dfrac{H\left(a+\frac{2i-2}{2}\Delta x\right)-H\left(a+\frac{2i-1}{2}\Delta x\right)}{H\left(a+\frac{2i-1}{2}\Delta x\right)-H\left(a+\frac{2i}{2}\Delta x\right)}<\dfrac{F\left(a+\frac{4i-1}{4}\Delta x\right)-F\left(a+\frac{4i-2}{4}\Delta x\right)}{F\left(a+\frac{4i-2}{4}\Delta x\right)-F\left(a+\frac{4i-3}{4}\Delta x\right)} : P_{m,1}<P_{m,2} \\ otherwise : P_{m,1}\geq P_{m,2}\end{cases} \tag{32}$$

where $\Delta x=\frac{b-a}{2^n}$.

4. Underestimation-overestimation boundary, with a small number of subintervals

For the seismic risk based on the midpoint level of the fragility curve, the ground motion level boundary at which the underestimation result was identified is in the convex region of the fragility curve. Per Eq. (32), the boundary can be derived by assuming the changes of each hazard term and fragility term to be the slope at the midpoint of each subinterval, per:

$$\frac{h\left(a+\frac{8i-6}{8}\Delta x\right)}{h\left(a+\frac{8i-2}{8}\Delta x\right)}\leq\frac{f\left(a+\frac{8i-3}{8}\Delta x\right)}{f\left(a+\frac{8i-5}{8}\Delta x\right)} \tag{33}$$

where $h(x)$ and $f(x)$ are the derivatives of the hazard and fragility curves, respectively.

The underestimation-overestimation boundary is based on the point at which the equation that shifts the right term to the left is less than 0. Applying Eqs. (2) and (3) enables the boundary equation, $y(i)$, to be derived per Eq. (34). If the equation is negative, the result will be underestimated when using a smaller number of subintervals.

$$y(i)=\left(\frac{a_1}{a_4}\right)^{-K_H-1}-\frac{a_2}{a_3}\exp\left(\frac{\ln\left(\frac{a_2}{a_3}\right)\ln\left(\frac{a_2a_3}{A_m^2}\right)}{2\beta_c^2}\right) \tag{34}$$

where $a_1=a+\frac{8i-6}{8}\Delta x$

$a_2=a+\frac{8i-5}{8}\Delta x$

$a_3=a+\frac{8i-3}{8}\Delta x$

$a_4=a+\frac{8i-2}{8}\Delta x$

The boundary equation can be solved by employing the false position method [34]. Fig. 1 gives a flowchart for finding the root of Eq. (34). To derive the boundary, this method requires the hazard data (K_I, K_H), fragility data (A_m,β_r,β_u), and error limit (EL). The entire ground motion level ranges from a to b, but the boundary is located in the convex region of the fragility curve, which is less than A_m. The false position method is based on the linear line that connects two points. The two initial points are i_1 and i_N, representing the initial ground motion level a and the median ground motion level capacity A_m. The second point i_2 is positioned where the initial line intersects the x-axis. The next point is then obtained as follows, after determining the location via the root of Eq. (34) with the root:

$$\begin{cases}y(i_k)y(i_N)<0 : i_{k+1}=\dfrac{i_k y(i_N)-i_N y(i_k)}{y(i_N)-y(i_k)} \\ y(i_k)y(i_N)>0 : i_{k+1}=\dfrac{i_1 y(i_k)-i_k y(i_1)}{y(i_k)-y(i_1)}\end{cases} \tag{35}$$

The false position method is performed until the change of i is below the error limit, thus indicating the boundary ground motion level, x_β. If the number of subintervals ($N=2^n$) falls under the predetermined threshold, it cannot be converged. Thus, the calculation is iterated by increasing n until the change in ground motion level boundary falls below the error limit.

5. Example of using the proposed method to derive the underestimation-overestimation boundary

This section provides an example in which a hazard curve with $K_I=$

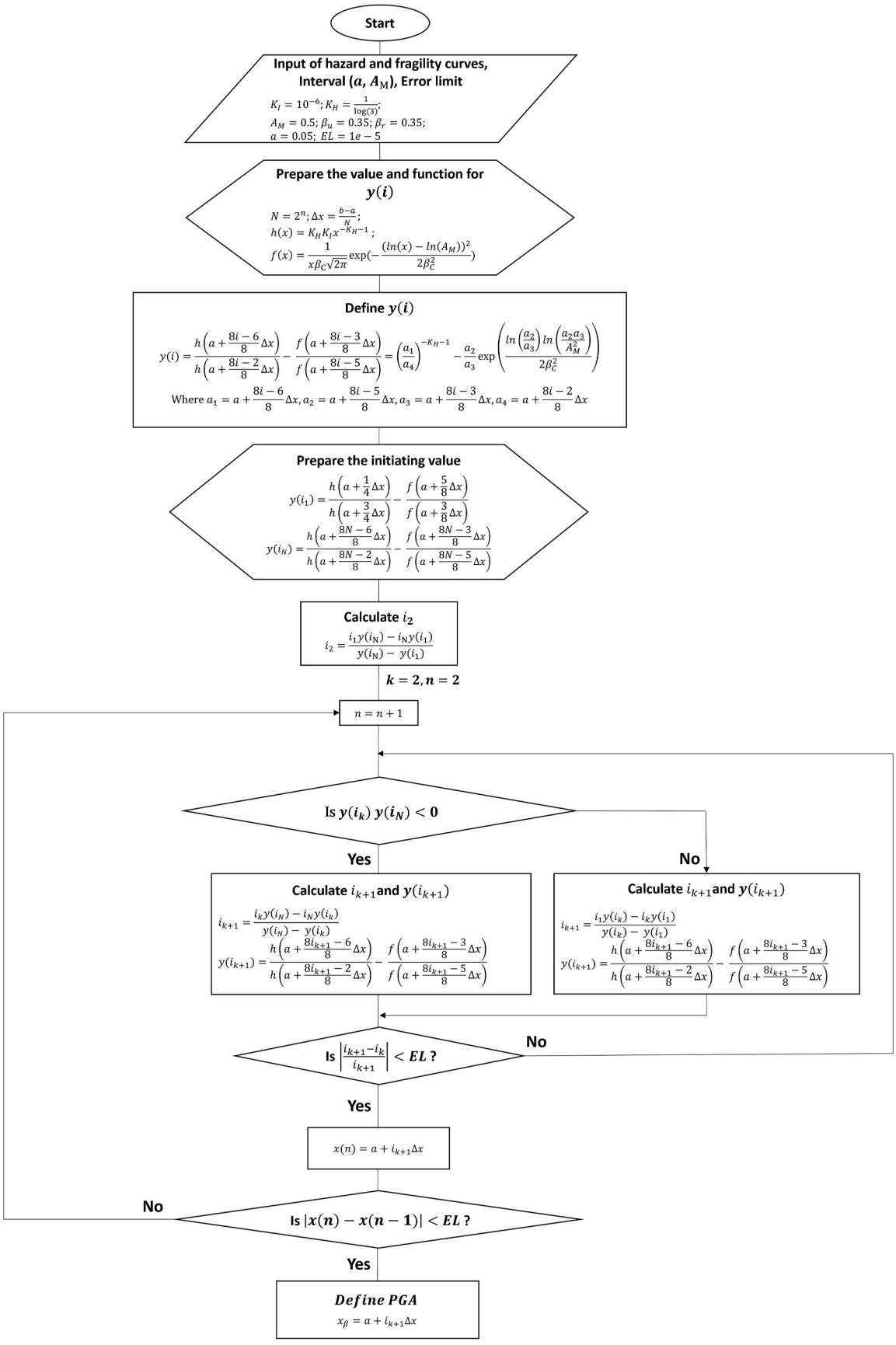

Fig. 1. False position method for finding the roots of $y(i)$.

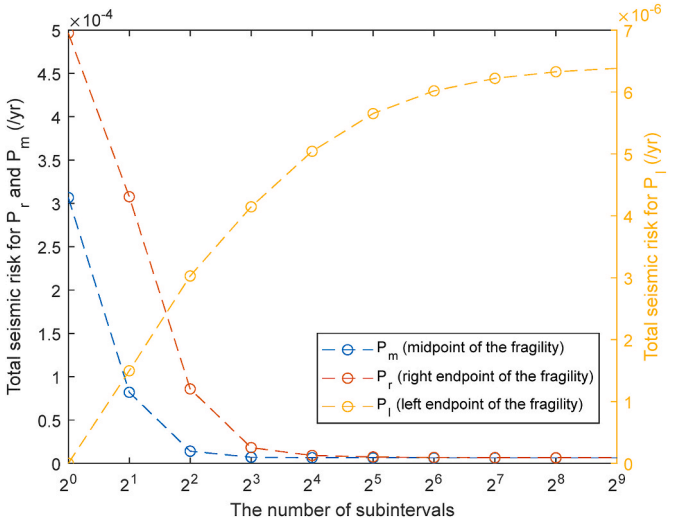

Fig. 2. Example of seismic risk, depending on the representative ground motion level of the fragility term.

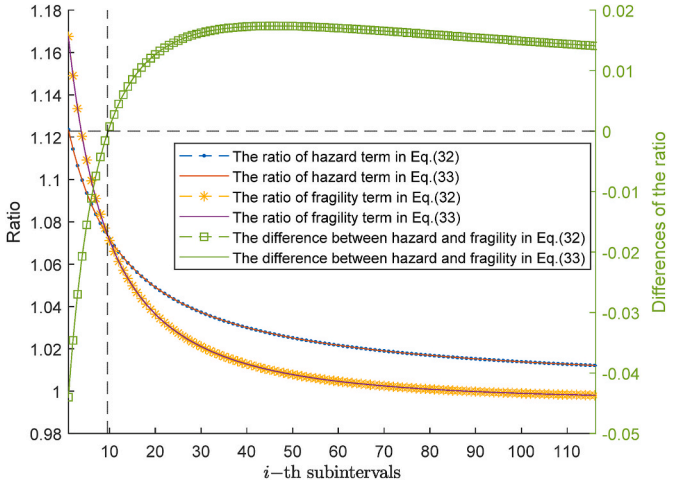

Fig. 3. Hazard and fragility terms in Eqs. (32) and (33).

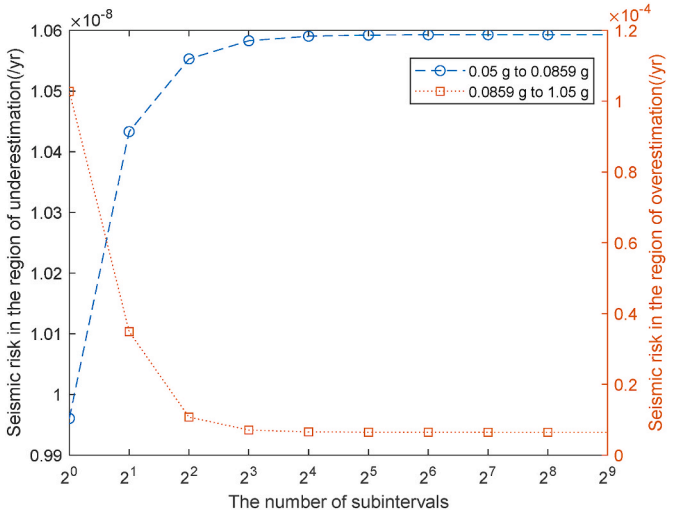

Fig. 4. Seismic risk for the two regions, depending on the number of subintervals.

10^{-6} and $(K_H) = 1/\ln(3)$, and a fragility curve with $A_M = 0.5$ and $\beta_u = \beta_r = 0.35$, are considered. The entire ground motion level was analyzed from 0.05 to 1.05 g, and the subintervals were divided into 2^8. Each subinterval was analyzed based on a ground motion level of $(a+(i-1)\Delta x)$ up to $(a + i\Delta x)$. Depending on whether the subinterval was analyzed as one section or two, a subinterval in which seismic risk is underestimated may occur as a result of a small number of subintervals.

Fig. 2 shows the seismic risk depending on the representative ground motion level of the fragility term. The risk based on the left endpoint is underestimated when using a small number of subintervals, whereas the risks based on the midpoint and right endpoint are overestimated. The results also show that the risk is converged with a large number of subintervals. Because, in practice, the number of subintervals is finite, it is recommended to conservatively use the right endpoint so as to prevent underestimation of the seismic risk.

When the midpoint is used, there exist ground motion levels where underestimation occurs if the number of subintervals is insufficient. This boundary can be identified from Eqs. (32) and (33), which incorporate both hazard and fragility data. Fig. 3 illustrates how the boundary depends on the ratios of the hazard and fragility term within each subinterval. The hazard and fragility terms illustrated by the dashed lines and markers represent the ratios of the hazard and fragility differences from a to A_m from Eq. (32). When illustrated by solid lines, the hazard and fragility terms indicate the ratios of the differentials of the hazard and fragility curves from Eq. (33). Because the dashed and solid lines are similar when Δx is small enough, we can use Eq. (33) to find the root. Fig. 3 also presents the differences between the hazard and fragility terms via the green line, which can be also defined by Eq. (34). In lower ground motion levels, the fragility term exceeds the hazard term in case where the difference of their ratios is negative. But as the difference of their ratios is positive, the relation of the hazard and fragility terms is reversed, and thus the risk cannot be underestimated. The point at which the difference of their ratios is zero is the underestimation-overestimation boundary, which depends on the number of subintervals. In this example, the boundary is located at around the 10-th subinterval, which represents a ground motion level of between 0.0852 and 0.0891 g.

The ground motion level boundary where Eq. (34) is positive can be determined as x_β when using the false position method described in Section 4. In this example, the ground motion level 0.0859 g can be obtained as x_β, with the error limit 10^{-5}. Fig. 4 represents the seismic risk depending on the number of subintervals for the two regions. The first region, with a ground motion level of between 0.05 and 0.0859 g is where underestimated results are obtained by using a smaller number of

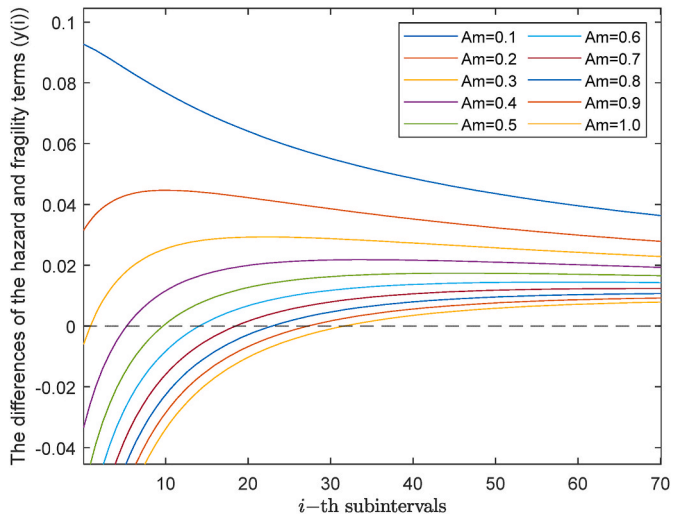

Fig. 5. Boundary equation, depending on A_M ($\beta_r = \beta_u = 0.35$).

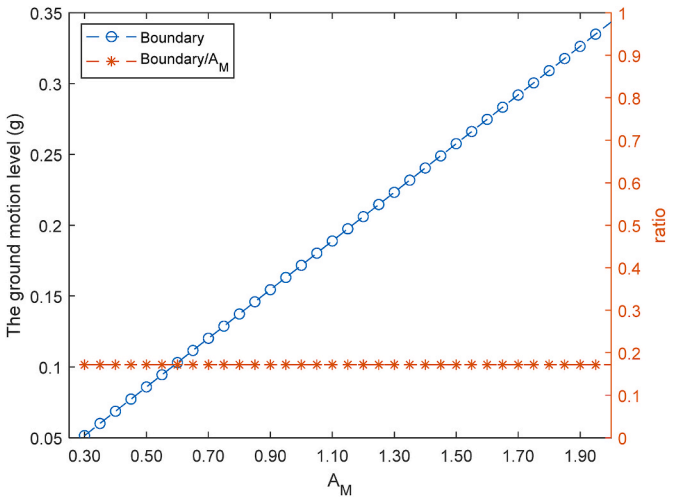

Fig. 6. Boundary ground motion level, depending on A_M ($\beta_r = \beta_u = 0.35$).

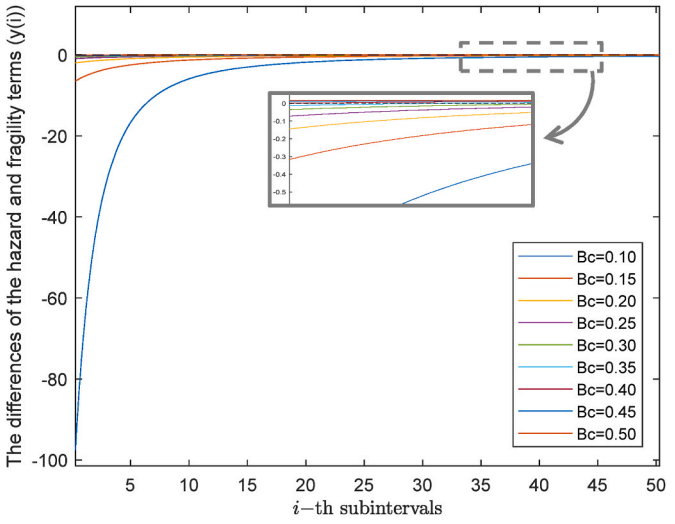

Fig. 7. Boundary equation, depending on β_c ($A_M = 0.5$).

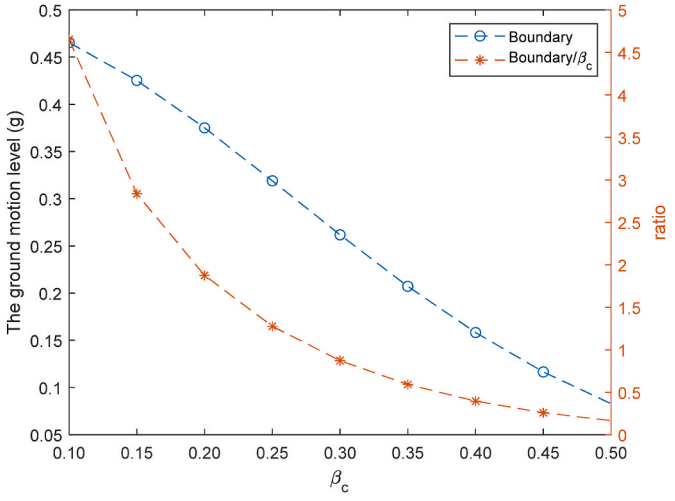

Fig. 8. Boundary ground motion level, depending on β_c ($A_M = 0.5$).

subintervals. The other region causes the risk to be overestimated as the number of subintervals decreases.

As seen in Figure, only a few regions lead to underestimated results when using a small number of subintervals. Most other subintervals, including the concave and even part of the convex region of the fragility curve, are more conservative when the number of subintervals is small. Additionally, in Figure, the seismic risk in the region which ranges from 0.0859 to 1.05 g greatly contributes to the seismic risk, which is also much wider. Thus, the total seismic risk with the midpoint representative level can at least be approximated based on conservative results, even using a small number of subintervals (see Fig. 2).

6. Discussion

The discrete approach to seismic quantification is based on making an assumption as to the representative ground motion level within each subinterval. With a finite number of subintervals being considered in practical application, assumption of the representative ground motion level can affect seismic risk estimates. At this point, the fact that using a small number of subintervals leads to underestimation of risk may be important to note. As discussed in Section 3, we were able to confirm that seismic risk is affected by the representative ground motion level. Although using the left endpoint the case in which the risk is based on the midpoint level leads to both overestimation and underestimation of risk depending on the ground motion level.

Additionally, it should be noted that, in practice, the hazard curve is typically not provided in a closed-form analytical expression, and the fragility curve is not represented by a single function [35]. However, since the hazard curve generally follows a monotonic decreasing trend [36], it has limited influence on whether underestimation or overestimation occurs for a given the representative ground motion level. In contrast, fragility data directly influences the curvature of the fragility curve, resulting in different convex and concave regions across the ground motion level. It can affect where the underestimation and overestimation occur with a smaller number of subintervals.

Therefore, the boundary equation, $y(i)$, was analyzed in accordance with the fragility data. Fig. 5 shows the boundary equation, and Fig. 6 shows the boundary ground motion level as per the change of A_M. In Fig. 5, the underestimation-overestimation boundary is based on the point that becomes 0. It can be shown that the boundary moves to the right as A_M increases. In other words, the lower A_M does not make the underestimation boundary. In cases where the value of A_M is low but has an underestimation boundary, such as 0.3 in Fig. 5, obtaining a reliable solution becomes challenging. To derive more accurate estimates of the boundary ground motion level, the false position method proposed in Section 4 can be employed. Fig. 6 illustrates the boundary ground motion level derived via the proposed method. The boundary ground motion level is also shown to increase as A_M increases. In addition, the boundary ground motion level is seen to be proportional to A_M, and the ratio of boundary ground motion level to A_M is constant.

Figs. 7 and 8 show the boundary equation and boundary ground motion level, respectively, in accordance with β_c. Unlike with A_M, it is difficult to see a consistent trend, but the boundary does appear in a lower ground motion level than for A_M. This indicates that a substantial number of subintervals is needed to avoid underestimation of risk when analyzing low ground motion levels.

7. Conclusions

The discrete approach is one of the most commonly used methods in seismic risk quantification, as it can be conducted similarly to the traditional PSA method, using standard PSA software. However, in practical applications, an infinite number of subintervals cannot be analyzed to obtain an exact result, so the seismic risk is approximated using a finite number of subintervals. In this approach, the representative ground motion level in each subinterval is also assumed to reflect

the hazard and fragility values for different ground motion levels. These assumptions, historically determined via expert judgment and without sufficient justification, have been applied to various different analytical practices.

The present study analyzed how representative ground motion level affects seismic risk when using a small number of subintervals. The hazard term does not affect the seismic risk value, because it applies the difference between the minimum and maximum values to the corresponding subinterval. However, the fragility curve does affect seismic risk because it applies the failure probability for one representative ground motion level. Accordingly, the left endpoint of the representative ground motion level was confirmed to be underestimated in a small number of subintervals, and the right endpoint was overestimated. When using the midpoint level, although it can depend on the hazard and fragility data, the underestimation-overestimation boundary was confirmed to occur in a lower ground motion level than for A_M, which is located in the convex region of the fragility curve. This article also proposed a method of deriving this boundary ground motion level.

The present study concluded that when the representative ground motion level is based on the left endpoint or midpoint level, it should be analyzed using a sufficient number of subintervals. This is because underestimation of seismic risk is something to be carefully considered, as significant contributions may be overlooked. This study adds to the current understanding of seismic risk quantification when using the discretization method, as well as the understanding of seismic risk changes in response to assumptions regarding such things as representative ground motion level and the number of subintervals. This study can provide a mathematical basis for selecting representative ground motion levels in seismic PSA, and can help seismic PSA analysts identify and prevent underestimation of risk.

Funding

This work was partly supported by the Korea Institute of Energy Technology Evaluation and Planning (KETEP) grant funded by the Ministry of Trade, Industry and Energy (MOTIE) of Republic of Korea [grant number RS-2024-00398867].

CRediT authorship contribution statement

Jisuk Kim: Writing – original draft, Methodology, Investigation, Conceptualization. **Man Cheol Kim:** Writing – review & editing, Supervision, Funding acquisition.

Declaration of competing interest

The authors declare that they have no known competing financial interests or personal relationships that could have appeared to influence the work reported in this paper.

Acknowledgements

Neither the U.S. Government, nor any agency thereof, nor any of their employees makes any warranty, express or implied, or assumes any legal liability or responsibility for the accuracy, completeness, or usefulness of any information, apparatus, product, or process disclosed, or represents that its use would not infringe on privately owned rights.

References

[1] M.C. Kim, Rigorous derivation of interfacing system LOCA frequency formulas for probabilistic safety assessment of nuclear power plants, Reliab. Eng. Syst. Saf. 238 (2023) 109470.
[2] G.S. Song, M.C. Kim, Comparison of state-of-knowledge correlation effect associated with lognormal, beta, and gamma uncertainty distributions, Reliab. Eng. Syst. Saf. 245 (2024) 110033.
[3] T. Zhou, M. Modarres, E.L. Droguett, Multi-unit nuclear power plant probabilistic risk assessment: a comprehensive survey, Reliab. Eng. Syst. Saf. 213 (2021) 107782.
[4] Y. Hu, T. Parhizkar, A. Mosleh, Guided simulation for dynamic probabilistic risk assessment of complex systems: concept, method, and application, Reliab. Eng. Syst. Saf. 217 (2022) 108047.
[5] R.G. Maidana, T. Parhizkar, A. Gomola, I.B. Utne, A. Mosleh, Supervised dynamic probabilistic risk assessment: review and comparison of methods, Reliab. Eng. Syst. Saf. 230 (2023) 108889.
[6] X. Zheng, H. Tamaki, T. Sugiyama, Y. Maruyama, Dynamic probabilistic risk assessment of nuclear power plants using multi-fidelity simulations, Reliab. Eng. Syst. Saf. 223 (2022) 108503.
[7] F. Antonello, J. Buongiorno, E. Zio, A methodology to perform dynamic risk assessment using system theory and modeling and simulation: application to nuclear batteries, Reliab. Eng. Syst. Saf. 228 (2022) 108769.
[8] R.J. Budnitz, Current status of methodologies for seismic probabilistic safety analysis, Reliab. Eng. Syst. Saf. 62 (1–2) (1998) 71–88, https://doi.org/10.1016/S0951-8320(97)00158-0.
[9] J. Sursock, Seismic Probabilistic Risk Assessment Implementation Guide, EPRI, 2013. https://www.epri.com/research/products/3002000709.
[10] T. Zhou, M. Modarres, E.L. Droguett, An improved multi-unit nuclear plant seismic probabilistic risk assessment approach, Reliab. Eng. Syst. Saf. 171 (2018) 34–47, https://doi.org/10.1016/j.ress.2017.11.015.
[11] H.K. Lim, A study of system analysis method for seismic PSA of nuclear power plants, J. Korean Surg. Soc. 34 (5) (2019) 159–166, https://doi.org/10.14346/JKOSOS.2019.34.5.159.
[12] J.D. Segarra, M. Bensi, M. Modarres, A bayesian network approach for modeling dependent seismic failures in a nuclear power plant probabilistic risk assessment, Reliab. Eng. Syst. Saf. 213 (2021) 107678.
[13] K. Kubo, K. Fujiwara, Y. Tanaka, Y. Hakuta, D. Arake, T. Uchiyama, K. Muramatsu, A scoping study on the use of direct quantification of fault tree using Monte Carlo simulation in seismic probabilistic risk assessments. 29th International Conference on Nuclear Engineering, 2022.
[14] S. Kwag, E. Choi, S. Eem, J.-G. Ha, D. Hahm, Toward improvement of sampling-based seismic probabilistic safety assessment method for nuclear facilities using composite distribution and adaptive discretization, Reliab. Eng. Syst. Saf. 215 (2021) 107809, https://doi.org/10.1016/j.ress.2021.107809.
[15] Y. Watanabe, T. Oikawa, K. Muramatsu, Development of the DQFM method to consider the effect of correlation of component failures in seismic PSA of nuclear power plant, Reliab. Eng. Syst. Saf. 79 (3) (2003) 265–279, https://doi.org/10.1016/S0951-8320(02)00053-4.
[16] J. Prochaska, P. Halada, M. Pellissetti, M. Kumar, Report 1: Guidance Document on Practices to Model and Implement Seismic Hazards in Extended PSA, vol. 2, ASAMPSA_E, 2016 (implementation in Level 1 PSA), https://asampsa.eu/wp-content/uploads/2014/10/ASAMPSA_E-D50.15-REPORT1-EARTHQUAKEPSAvol-2.pdf.
[17] IAEA, Probabilistic Safety Assessment for Seismic Events, International Atomic Energy Agency, 2020. https://www.iaea.org/publications/14744/probabilistic-safety-assessment-for-seismic-events.
[18] USNRC, Risk Assessment of Operational Events Handbook (Volume 2-external Events), U.S. Nuclear Regulatory Commission, 2017. https://www.nrc.gov/docs/ML1734/ML17349A301.pdf.
[19] S.H. Han, A hybrid approach of partially applying BDD for seismic PSA quantification, Nucl. Eng. Technol. 56 (10) (2024) 4289–4295, https://doi.org/10.1016/j.net.2024.05.034.
[20] S.K. Park, W.S. Jung, Probability subtraction method for accurate quantification of seismic multi-unit probabilistic safety assessment, Nucl. Eng. Technol. 53 (4) (2021) 1146–1156, https://doi.org/10.1016/j.net.2020.09.022.
[21] W.S. Jung, A method to avoid underestimated risks in seismic SUPSA and MUPSA for nuclear power plants caused by partitioning events, Energies 14 (8) (2021) 2150, https://doi.org/10.3390/en14082150.
[22] J.S. Kim, M.C. Kim, Insights gained from applying negate-down during quantification for seismic probabilistic safety assessment, Nucl. Eng. Technol. 54 (8) (2022) 2933–2940, https://doi.org/10.1016/j.net.2022.03.014.
[23] J.S. Kim, M.C. Kim, Development of a software tool for seismic probabilistic safety assessment quantification with a sufficiently large number of bins for enhanced accuracy, Energies 14 (6) (2021) 1677, https://doi.org/10.3390/en14061677.
[24] J.S. Kim, M.C. Kim, The effect of the number of subintervals upon the quantification of the seismic probabilistic safety assessment of a nuclear power plant, Nucl. Eng. Technol. 55 (4) (2023) 1420–1427, https://doi.org/10.1016/j.net.2022.12.030.
[25] R.P. Kassawara, Surry Seismic Probabilistic Risk Assessment Pilot Plant Review, EPRI, 2010. https://www.epri.com/research/products/000000000001020756.
[26] TVA, Sequoyah nuclear plant (SQN) units 1 and 2 seismic probabilistic risk assessment in response to 50.54(f, Letter with Regard to NTTF 2.1 Seismic PRA Summary Report (2019). https://www.nrc.gov/docs/ML1929/ML19291A003.pdf.
[27] PG&E, Diablo Canyon Power Plant Seismic Probabilistic Risk Assessment Summary Report, Pacific Gas & Electric Company, U.S. Nuclear Regulatory Commission, 2018. https://www.nrc.gov/docs/ML1812/ML18120A201.pdf.
[28] M. Kohrangi, P. Bazzurro, D. Vamvatsikos, A. Spillatura, Conditional spectrum based ground motion record selection using average spectral acceleration, Earthq. Eng. Struct. Dynam. 48 (9) (2019) 1066–1082, https://doi.org/10.1002/eqe.2946.
[29] B. Li, Z. Cai, Z. Duan, Selection of hazard-consistent ground motions for risk-based analyses of structures, Struct. Saf. 104 (2023) 102365, https://doi.org/10.1016/j.strusafe.2023.102365.
[30] R. Kennedy, S.A. Short, Basis for Seismic Provisions of DOE-STD-1020, U.S. Department of Energy, 1994, https://doi.org/10.2172/10146835.

[31] R.P. Kennedy, Overview of methods for seismic PRA and margin analysis including recent innovations. Proceedings of the OECD-NEA Workshop on Seismic Risk, 1999. Tokyo, Japan.
[32] R. Kennedy, M. Ravindra, Seismic fragilities for nuclear power plant risk studies, Nucl. Eng. Des. 79 (1) (1984) 47–68, https://doi.org/10.1016/0029-5493(84)90188-2.
[33] T. Uchiyama, K. Kawaguchi, T. Wakabayashi, Effect of analytical methodology for assessment on seismically induced core damage, J. Power Energy Syst. 5 (3) (2011) 279–294, https://doi.org/10.1299/jpes.5.279.
[34] R.L. Burden, J.D. Faires, A.M. Burden, Numerical Analysis, Cengage Learning, 2015.
[35] O.S. Bursi, R. Filippo, V.L. Salandra, M. Pedot, M.S. Reza, Probabilistic seismic analysis of an LNG subplant, J. Loss Prev. Process. Ind. 53 (2018) 45–60, https://doi.org/10.1016/j.jlp.2017.10.009.
[36] C. Scawthorn, W.F. Chen, Earthquake Engineering Handbook, Talyor & Francis, 2002.
[37] S. Kwag, E. Choi, D. Hahm, M. Kim, S. Eem, Computationally efficient complete-sampling-based fault tree analyses for seismic probabilistic safety assessment of nuclear facilities, Expert Syst. Appl. (2025) 125341., https://doi.org/10.1016/j.eswa.2024.125341.